Control of Thermal and Electronic Transport in Defect-Engineered Graphene Nanoribbons

Justin Haskins,[†] Alper Kınacı,[‡] Cem Sevik,[†] Hâldun Sevinçli,[§] Gianaurelio Cuniberti,[§,⊥,*] and Tahir Çağın[†,*]

[†]Artie McFerrin Department of Chemical Engineering, and [‡]Material Science and Engineering, Texas A&M University, College Station, Texas 77845-3122, United States, [§]Institute for Materials Science and Max Bergmann Center of Biomaterials, Dresden University of Technology, 01062 Dresden, Germany, and [⊥]Division of IT Convergence Engineering and National Center for Nanomaterials Technology, POSTECH,Pohang 790-784, Republic of Korea

ABSTRACT The influence of the structural detail and defects on the thermal and electronic transport properties of graphene nanoribbons (GNRs) is explored by molecular dynamics and non-equilibrium Green's function methods. A variety of randomly oriented and distributed defects, single and double vacancies, Stone–Wales defects, as well as two types of edge form (armchair and zigzag) and different edge roughnesses are studied for model systems similar in sizes to experiments (>100 nm long and >15 nm wide). We observe substantial reduction in thermal conductivity due to all forms of defects, whereas electrical conductance reveals a peculiar defect-type-dependent response. We find that a 0.1% single vacancy concentration and a 0.23% double vacancy or Stone–Wales concentration lead to a drastic reduction in thermal conductivity of GNRs, namely, an 80% reduction from the pristine one of the same width. Edge roughness with an rms value of 7.28 Å leads to a similar reduction in thermal conductivity. Randomly distributed bulk vacancies are also found to strongly suppress the ballistic nature of electrons and reduce the conductance by 2 orders of magnitude. However, we have identified that defects close to the edges and relatively small values of edge roughness preserve the quasi-ballistic nature of electronic transport. This presents a route of independently controlling electrical and thermal transport by judicious engineering of the defect distribution; we discuss the implications of this for thermoelectric performance.

KEYWORDS: thermal transport · electronic transport · thermoelectric · graphene · carbon

Low-dimensional carbon-based nanomaterials, graphene[1,2] and graphene nanoribbons (GNRs), have attracted extensive attention in recent years due to their extraordinary electrical,[3−7] optical,[8,9] thermal,[10−14] and mechanical[15,16] properties. The experimental room temperature (RT) carrier mobility (15 000−27 000 $cm^2 V^{-1}s^{-1}$), quantized electrical conductance, high Seebeck coefficient,[17] extremely high RT thermal conductivity (κ) of graphene, and the ability to tune these properties by changing width and edge structure[18−21] have motivated many scientists to consider graphene-based materials for future nanoscale device applications,[22−25] including thermal management in nanoelectronics[26,27] and thermoelectric power generation.[28−32] Recent developments in fabrication techniques have made it possible to grow very narrow[33,34] and atomically precise[35] GNRs, further stimulating interest in this direction.

The room temperature thermal conductivity of graphene has been measured by several groups, and reported values range between 400 and 600 W/mK[10,13] and 2500−5300 W/mK[11−13] for the supported and suspended samples, respectively. The strong dependence of these values on the length and width of the samples can be attributed to the long RT phonon mean free path (MFP), which is reported to be around 750 nm.[26] In addition to these experimental studies, a substantial theoretical effort based on several different techniques has been devoted to understand the thermal transport properties of both graphene[36−39] and GNRs.[40−49] The calculations confirm the experimentally predicted high values for κ at RT, particularly for the suspended graphene, and support the observed effects of width and length on thermal transport. Additionally, significant variations in κ of GNRs with edge termination have been predicted, where zigzag GNRs (ZGNRs) are found to be thermally more conductive than the armchair GNRs (AGNRs) having the same width and length.[40,43,45,50,58] In spite of this serious theoretical effort, the effects of intrinsic defects, single and double vacancies, topological defects, edge termination, and level of roughness on κ of experimentally feasible GNRs have not been systematically studied as of yet. In particular, the extensive investigation of how these imperfections can be used to tune the resulting thermal transport would be enormously beneficial for future technological applications of GNRs.

On the other hand, the influence of these imperfections on the electronic transport is not parallel to the thermal case. The electronic

* Address correspondence to g.cuniberti@tu-dresden.de, tcagin@che.tamu.edu.

Received for review January 11, 2011 and accepted March 31, 2011.

Published online March 31, 2011
10.1021/nn200114p

transport can exhibit surprising variations that depend on the type of defects, chirality, and edge structure.[7,28,51−57] While edge roughness produces a decrease in the thermal transport through GNRs regardless of the chirality or width,[28,48,58] its effect on electronic transport is more complex. The electronic transport through edge-roughened ZGNRs retains the quasi-ballistic transport characteristics of pristine GNRs;[7,28,51,59] however, the quasi-ballistic nature of AGNRs is deteriorated significantly by the presence of only minute edge disorder.[7,51,54,56] On the other end of the spectrum, bulk vacancies have been shown to reduce both the thermal and electronic transport at small concentrations, independent of the ribbon chirality.[52,60,61] ZGNRs are of particular interest due to the fact that electrons in the first conduction plateau (FCP) are less sensitive to edge disorder, where phonons are strongly suppressed. This opposite behavior can give rise to a thermoelectric figure of merit (*ZT*) as high as 4 at room temperature.[28] The principal aim of this study is to analyze the interplay between defects in GNRs and the resulting effects on thermal and electronic transport. We investigate each of these cases meticulously to obtain a better understanding of the transport properties and the possible independent control of them for potential applicability of GNRs as thermoelectrics. The findings then can be used as guide for future experimental and theoretical work.

RESULTS AND DISCUSSION

Thermal Transport. The effect of randomly distributed single and double vacancies, Stone−Wales defects, and ribbon-edge terminations and level of roughness on the κ of GNR structures having a width of >15 nm and a length of >100 nm are considered in this study. This requires simulations of systems (up to 300 000 atoms) that have experimental dimensions with rough edges and various structural defects, each of which affects thermal conductivity and the electronic properties differently. Figure 1 shows various structural aspects of GNRs that are investigated in this work, including rough edges, single vacancies, double vacancies, and Stone−Wales defects. To perform the lattice thermal conductivity calculations, we employ molecular dynamics and Green−Kubo formalism (see the Methods section). A reoptimized Tersoff parameter set[38] (RP) is used to represent graphene and GNRs. The original Tersoff parameter set[62] (OP) underestimates the frequencies of the acoustic phonon modes, while the RP produces a graphene phonon dispersion in good agreement with experiment. Of fundamental importance is that the RP captures the quadratic behavior of the lowest frequency phonon modes near the Γ point. The OP produces linear behavior in this region, which may cause significant error in thermal conductivity. The significance of this difference is reflected by a 50−60% underestimation

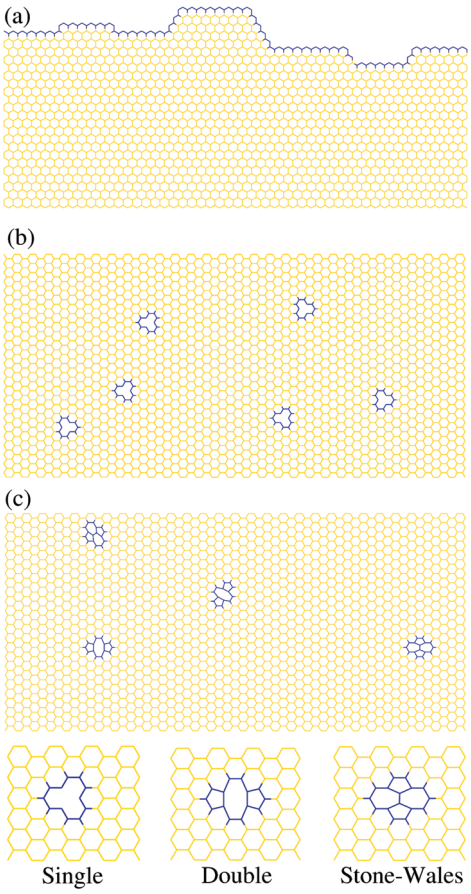

Figure 1. Schematic description of graphene nanoribbons including (a) edge defects, (b) single vacancies, (c) Stone−Wales defects and double vacancies.

of the thermal conductivity of graphene by the OP when compared to the RP (Figure 2a). As a further note, the RT κ produced by the RP, 2600 W/mK, is coherent with various experimental measurements and theoretical calculations.[10,12,38,63] The slope of the lattice thermal conductivity shows a decreasing trend with temperature due to an increase in phonon population at higher energy states, resulting in an increase in phonon scattering.

Before discussing how edge and vacancy defects affect the κ of GNRs, it is important to thoroughly understand the behavior of the pristine GNRs, including how the length of the simulated GNR influences the resulting thermal conductivity. Certain artificial size effects can arise in MD due to the periodic boundary conditions along the transport direction for the nanosystems. When the simulation size is too small for a nanosystem simulated using 1D or 2D periodicity, this periodicity leads to correlated scattering events which reduce the calculated thermal conductivity, requiring a systematic study of length dependence.[64] A variety of studies have reached different conclusions on what dimension is sufficient for a GNR to be free from these spurious size effects, but most use a length on the order of tens of nanometers.[40] The length dependence of κ (see Figure 2b) suggests that the minimum length to attain a converged κ value should be

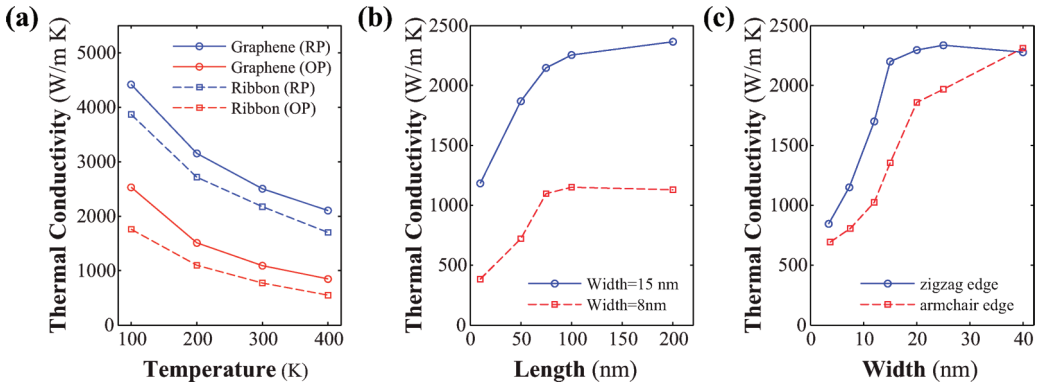

Figure 2. Lattice thermal conductivity of (a) graphene calculated with both original (OP) and reoptimized (RO) empirical interatomic potentials, (b) ZGNRs having widths of 15 and 8 nm and lengths up to 200 nm, (c) ZGNRs and AGNRs having lengths of 100 nm and widths up to 40 nm. All simulations are at ambient conditions unless noted otherwise.

around 75−100 nm, as reflected in the results for ZGNRs with widths of 15 and 8 nm. At this limit, the RT κ for a 15 nm wide ZGNR is shown to reach 2300 W/mK. The ribbon width also produces a strong effect that can clearly be seen for both ZGNRs and AGNRs (Figure 2c). At a width of 4 nm, κ becomes quite small, 840 and 680 W/mK for ZGNRs and AGNRs, respectively, and the edge scattering becomes more pronounced. With increasing width values, the κ of both edge termination forms steadily rises, with the zigzag termination form always remaining higher, nearly twice that of the armchair value at 15 nm width. The low value of κ for the AGNRs is a result of its higher number of edge scatterers compared to the ZGNRs; that is, the armchair termination has more atoms per unit length than the zigzag termination, which effectively increases the influence of the edges on κ. This persists until the width reaches 40 nm, after which the κ of both edge forms appears to converge to 2300 W/mK. This value is still 10% less than "infinite" graphene, suggesting that the approach to the graphene conductivity is gradual and requires much larger widths.

As evident from the difference in thermal conductivity of ZGNRs and AGNRs, the edge form/structure is a degree of freedom in modifying the thermal transport. Edge, in principle, is an extended defect and hence decreases the thermal conductivity. Roughness is another edge structure parameter that further modifies the average phonon mean free path by introducing additional scattering processes. In this study, the rough ribbon edges are randomly created with a target roughness value, and the coordination number is at least 2 for the edge carbon atoms. Naturally, for a higher roughness, there are more two-coordinated atoms for the ZGNRs. In Figure 1, a portion of one such ribbon edge with a roughness of 7.28 Å is shown. The thermal conductivity of the ribbon decreases with increasing roughness, as can be seen in Figure 3a. At room temperature, compared to smooth-edged ribbon of the same size, approximately an 80% reduction in the thermal conductivity

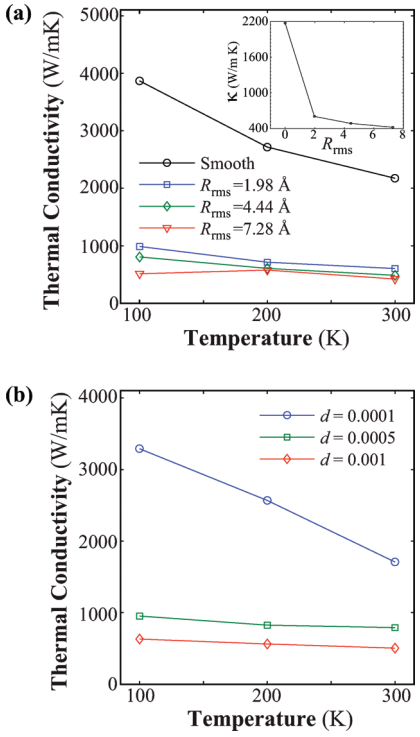

Figure 3. Temperature dependence of lattice thermal conductivity of (a) smooth/rough and (b) vacancy introduced ZGNRs. Three different roughness values (*i.e.*, 1.98, 4.44, and 7.28 Å) are considered. The rough ribbons are built such that they have the same number of atoms and length as a smooth ribbon of 500 nm long and 15 nm wide (the details of the algorithm used for generating rough edges is given in the Methods section). The inset shows the reduction of room temperature thermal conductivity as roughness is increased. Single vacancies are also introduced in a 500 nm long and 15 nm wide ribbon with three different concentrations: 0.0001, 0.0005, and 0.001.

value is observed for the highest roughness value. In addition, the data in Figure 3 show a drastic change in temperature dependence of κ. As the roughness increases, the slope of the conductivity curve approaches zero, indicating dominance of the scattering due to roughness. An analogous observation can be made as the single vacancy concentration is increased to 0.05%

TABLE 1. Thermal Conductivity Results for Various Defected ZGNRs of 100 nm Length and 15 nm Width at Ambient Conditions (Percent Decrease from the Pristine Case Is Also Included)

type	concentration	κ (W/mK)	% decrease
pristine		2300	
single vacancy	0.0001	1726	25
	0.0005	943	59
	0.0010	426	81
double vacancy	0.0010	707	69
Stone–Wales	0.0010	709	69
mix 50/50	0.0010	703	69
	0.0017	612	73
	0.0023	431	81

and above (see Figure 3b). The conductivity behaves much like defect-free ribbon for a vacancy concentration of 0.0001; however, the curve flattens when the vacancy concentration increases to 0.001. It is also noteworthy that, in extreme defect states, a very weak temperature-dependent behavior is observed with similar conductivity values.

For a more complete understanding of thermal transport in GNRs, the interplay between internal defect states and κ should be further addressed. We focus on the three most common types of defects, shown in Figure 1: single vacancies, double vacancies, and Stone–Wales defects. A single vacancy, removal of one atom, is a high energy defect that leaves three carbon atoms two-coordinated, effectively breaking the sp^2 character of the local lattice. A double vacancy, removal of two atoms from the lattice, is more favorable than a single vacancy as the local structure rearranges to restore the three-coordinated sp^2 bonding to each atom by creating an octagon and two pentagon structure. Similarly, a Stone–Wales defect is a topological defect that preserves sp^2 bonding by forming a structure with two heptagons and two pentagons. Among the defect types we consider, the single vacancy has the most dramatic effect on κ (Table 1). At very low concentrations, 0.0001 (corresponding to removal of 1 carbon atom out of 10 000), a 25% reduction in thermal conductivity is noted, while a concentration of 0.001 shows close to an 80% decrease from the values obtained for the pristine GNRs. However, a concentration of 0.001 for Stone–Wales and divacancies only reduces the thermal conductivity by 70%. To reach the 80% reduction, these concentrations must be increased to 0.0023. The underlying mechanism making single vacancies much more effective at reducing lattice thermal conductivity is intrinsically related to their less stable two-coordinated atoms. The two-coordinated atoms will be less likely to follow the normal pattern of vibrations in the pristine material and cause a higher degree of scattering. This point is further supported by the fact

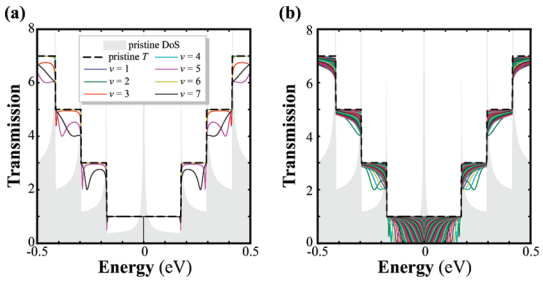

Figure 4. Electronic transmission through ZGNR(70) with a single vacancy located at various sites, *v*. The states within the first conduction plateau are weakly affected when the vacancy is close to the edges, $v \leq 7$ ($v = 1$ denoting the outermost atom) (a), but the quality is not preserved when the vacancy is positioned closer to the middle, $v > 7$ (b). The shaded regions are for the density of states of the pristine ribbon, and the dashed lines indicate the pristine transmission.

that the double vacancy and Stone–Wales defects have the same effect on thermal conductivity, and both have only sp^2 bonds. Even when Stone–Wales defects and double vacancies are mixed in a 1:1 ratio, the thermal conductivity remains the same as the pure double vacancy or Stone–Wales structure with the same concentration (Table 1). This weaker dependence of κ on the Stone–Wales defects has also been noted for single-wall carbon nanotubes and SWCNT bundles.[64]

Electronic Transport and Thermoelectric Properties. First, we investigate electronic transport through ZGNRs as a function of the spatial distribution of single vacancy defects. We perform the calculations for ZGNR(70), with 70 being the number of zigzag chains along the ribbon, which corresponds to a width of ~15 nm. There are 140 atoms per unit cell, and 70 inequivalent vacancy positions ($v = 1, ..., 70$). The electronic transmission ($\mathcal{T}_v$) in the presence of a single vacancy varies strongly depending on its position, *v* (see Figure 4). If the vacancy is located within 7.5 Å of the edge of the ZGNR ($v \leq 7$), the electronic states within the FCP are weakly affected, but edge-localized states at the charge neutrality point (CNP) are scattered strongly (Figure 4a). This is due to the fact that these edge states give rise to a singularity in the density of states (DOS) at the CNP[65] and are therefore prone to defects located close to the edges. The opening of a transport gap at the CNP and quasi-ballistic behavior within the FCP were reported previously for ZGNRs with edge roughness,[7,51] but to the best of our knowledge, similar behavior for vacancies close to the edges has not been reported before. As the single vacancy is positioned away from the edge ($v > 7$), states within the FCP are also scattered strongly (Figure 4b).

To better understand the electronic transport through defected GNRs, we investigate long ZGNRs with random distributions of single vacancies. Having obtained the transmission spectra of individual scatterers, we employ scattering theory which yields accurate results for dilute scatterers.[66,67] In the diffusive

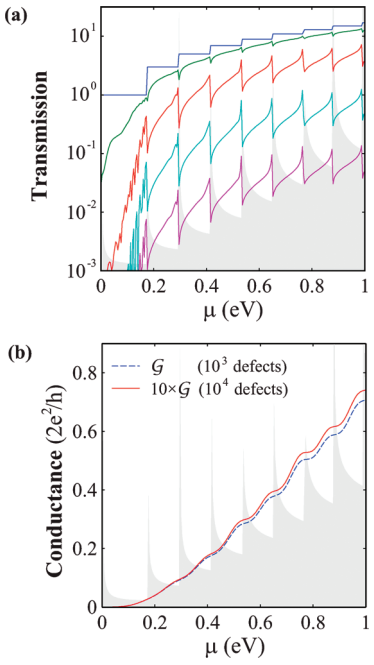

Figure 5. (a) Transmission spectra with a varying number of single vacancies with N = 0, 10, 100, 1000, and 10 000 in a 17.5 μm long ZGNR. (b) Room temperature electrical conductance $\mathcal{G}$ for $N = 10^3$ and $N = 10^4$ single vacancies (solid and dashed curves, respectively). For $N = 10^4$, conductance is reduced by approximately 1 order of magnitude compared to the $N = 10^3$ case (note the prefactor 10 in the legend), but quantum conductance plateaus are still distinguishable.

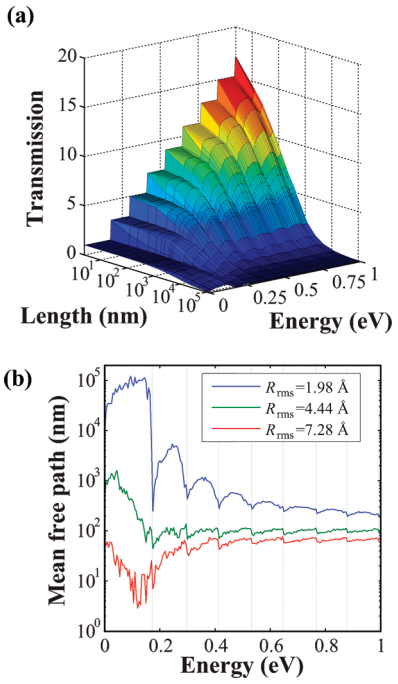

Figure 6. (a) Electron transmission for ZGNR(70) with edge roughness, R_{rms} = 1.98 Å, at lengths ranging from 0.25 nm (pristine case) to 125 μm. (b) Elastic mean free paths due to edge roughness are shown for different roughness values. Vertical gray lines in (b) indicate the band edges of pristine ZGNR(70).

regime, the resistance due to each scatterer is additive; therefore, the transmission due to N vacancies is obtained according to

$$\frac{1}{\mathcal{T}_N} = \frac{1-N}{\mathcal{T}_o} + \sum_v \frac{N_v}{\mathcal{T}_v}, \qquad (1)$$

where $R_o/2\mathcal{T}_o$ is the contact resistance, $\mathcal{T}_o$ is the pristine transmission and $R_o = h/e^2$ is the quantum of resistance. $\mathcal{T}_v$ and N_v are the transmission amplitude and the number of vacancies with particular configuration v, respectively, and $N = \Sigma_v N_v$ is the total number of vacancies in a sample. In Figure 5a, transmission spectra are plotted for different numbers of single vacancies ranging between $N = 10^1$ and 10^4 as well as that of the pristine ribbon. Here, $N = 10^4$ corresponds to a ZGNR of length, L, 17.5 μm with a defect concentration of d = 0.001. We note that the transmission spectrum is symmetric around the CNP (E = 0) due to electron hole symmetry of the Hamiltonian (see Methods). Single vacancies are most effective within the FCP, and sawtooth-like transmission profiles are observed for all N. We also calculate the room temperature electronic conductance for $N = 10^3$ and $N = 10^4$ (Figure 5b). We note that the conductance is reduced by more than 2 orders of magnitude for $N = 10^4$, compared to the pristine ZGNR, but the conductance plateaus are still observable. Survial of conductance plateaus, even when conductance is suppressed dramatically, was measured previously.[61] In a previous study, the emergence of the plateaus was assigned to be due to the enhanced backscattering by bulk vacancies.[60] In that work, the calculations were carried out for AGNRs, and sawtooth-like transmission profile for bulk disorder was observed, similar to the profiles we observe for ZGNRs. Our calculations show that the survival of the conductance steps are independent of the edge shape being armchair or zigzag.

As an important step to better understand electronic transport in GNRs, we investigate how the degree of edge roughness affects both electronic transmission through the ribbon and the mean free path of the electrons. For a ZGNR with edge roughness, we employ a recursive Green's function scheme.[68] We prefer the recursive scheme in order to include the multiple scattering effects due to the correlated and dense nature of edge roughness disorder. We calculate the transmission values of ZGNR(70) with edge roughness for various lengths of structures up to ~0.5 μm (2000 unit cells). In Figure 6a, we plot the electronic transmission values for sample lengths up to L = 125 μm with edge roughness R_{rms} = 1.98 Å. The transmission values for $L \leq 0.5$ μm are obtained by averaging over 25 representative structures of the desired edge roughness, as defined by the same algorithm in Figure 3. For $L > 0.5$ μm, we use the elastic mean free paths $\ell(E)$ to predict the transmission values. The mean free paths are obtained from the ensemble-averaged transmission spectra using $\mathcal{T}(E,L) = \mathcal{T}_p(1 + L/\ell(E))^{-1}$,

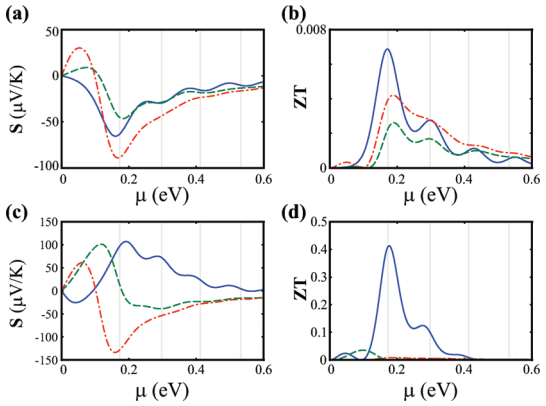

Figure 7. Seebeck coefficients are shown at T = 300 K for roughness values R_{rms} = 1.98 Å (solid), R_{rms} = 4.44 Å (dashed), and R_{rms} = 7.28 Å (dot-dashed) at lengths of L = 61.5 nm (a) and L = 125 μm (c). Thermoelectric figure of merit for the same set of parameters as (a) and (c) are given in (b) and (d), respectively. Vertical gray lines indicate the band edges of pristine ZGNR(70).

where $\mathcal{T}_p$ is the transmission of the pristine ribbon. In Figure 6a, one observes that transmission drops rapidly with length, except for the energy values E < 0.17 eV, and the reduction is more rapid for higher energies. This suppression is clearly visible in the energy dependence of ℓ in Figure 6b. For R_{rms} = 1.98 Å, ℓ is always longer than 10 μm within the FCP (E < 0.17 eV), reaching a value of 100 μm, then dropping rapidly with increasing energy and making dips at the band edges. The ℓ is shorter for higher R_{rms} at all energies. It is still considerably larger in the FCP compared to the rest of the spectrum for R_{rms} = 4.44 Å, but this behavior is reversed when R_{rms} = 7.38 Å. We assign this behavior to the fact that transmission within the FCP is preserved only when vacancies are within 7.5 Å of the edge ($v \leq 7$). In other words, when R_{rms} increases to 7.38 Å, the amplitude of the roughness can breach the 7.5 Å region at the edge, causing significant scattering in the FCP.

Comparing edge roughness with bulk vacancies, we note the destructive nature of bulk vacancies at low energies, while the quasi-ballistic transport through rough ZGNR with small R_{rms}, together with depressed lattice thermal conductivity of these structures, implies good thermoelectric properties. Indeed, as the length of the ribbon is increased, the ratio of phonon contribution to thermal conductance to the electron contribution is reduced. At room temperature, when R_{rms} = 1.98 Å and the chemical potential is pinned to the CNP, σ_{ph}/σ_{el} becomes 20.6, 2.3, and 0.3 for samples of lengths L = 0.25, 2.5, and 25 μm, respectively. In Figure 7a,c, we plot the Seebeck coefficients at T = 300 K for L = 61.5 nm and L = 125 μm, respectively. Local extrema of Seebeck coefficients, when the chemical potential is close to μ = 0.17 eV, are due to the rapid variation of the transmission function at the band edge, and R_{rms} = 1.98 Å yields the highest magnitude for all samples at all temperatures considered. For L = 61.5 nm, ZT is always lower than 10^{-2}. It increases with length and reaches the value of ZT = 0.41 for R_{rms} = 1.98 Å when L = 125 μm. Despite the fact that lattice thermal conductivity is lower for R_{rms} = 4.44 and 7.98 Å, such high ZT values are not observed for R_{rms} values larger than 1.98 Å. Again, this can be attributed to the suppressed electrical conductance for large R_{rms}.

CONCLUSION

The electronic and thermal properties of GNRs are strongly dependent on the dimensions of the structure, edge termination/roughness, and lattice defect distribution. In this study, molecular dynamics and non-equilibrium Green's function methods are utilized on GNRs of sizes up to micrometers in order to investigate the extent of these dependencies. Classical dynamics calculations show that decreasing the width, changing the termination of ribbons from zigzag to armchair, and roughening the edge all reduce the thermal conductivity due to an increase in the ratio of edge length to surface area. As this ratio increases, phonon edge scattering dominates the thermal behavior. Interestingly, the κ calculated for the roughest ribbon and the ones calculated for highest concentration of single vacancy, double vacancy, and Stone–Wales defects are all similar. Moreover, at these "extreme" concentration cases, κ behaves almost independent of the temperature, which is attributed to the defect-induced domination of elastic mean free paths over anharmonic mean free paths. Although the thermal conductivities of all the defected ribbons converged to similar values, the concentrations corresponding to these points are not all the same for internal defects. Single vacancies are more effective in decreasing κ compared to double vacancies and Stone–Wales defects. In fact, double vacancies and Stone–Wales defects do not show any quantitative difference.

Another dramatic difference between the effects of edge and bulk vacancies on the electronic conduction of ZGNRs suggests that bulk vacancies destroy the ballistic electronic transport properties of GNRs except when present within 7.5 Å of the edge. Despite the destruction of ballistic behavior by bulk defects, quantum conduction plateaus are still observable at low conductance values. Additionally, the electronic quality of ZGNRs with edge disorder can be preserved, provided that the edge roughness does not significantly breach the key 7.5 Å edge region. The weak dependence of electrical conduction on the edge roughness in ZGNRs is attributed to the fact that the electronic band within the first conduction plateau is only weakly dependent on the ribbon width, which is a characteristic of zigzag edge shape. Combined with

the suppressed lattice thermal conduction, edge-disordered ZGNRs have significant thermoelectric potential, while bulk defects suppress the thermoelectric quality.

METHODS

In order to calculate thermal conductivity, an accurate description of phonon dispersions, especially those of acoustic modes, of the considered material is extremely important as they strongly influence thermal transport properties.[69] Lindsay *et al.*[38] have recently shown that the original Tersoff[62] and Brenner-type empirical interatomic potential parameters do not accurately reproduce the phonon dispersions or the group velocities of the three acoustic branches. They have also presented a reoptimized parameter set which, for suspended graphene and (10,10) single-wall carbon nanotubes, gives a κ in much better agreement with the experimental results. In this study, the reoptimized parameter set is employed to accurately represent the phonons in graphene-based systems.[38]

Green–Kubo theory[70] is a standard technique used in equilibrium molecular dynamics simulations for the determination of transport coefficients through the time-integrated autocorrelation functions relevant to the targeted transport property, as dictated by the fluctuation–dissipation theorem. The correlation function approach is equivalent to time evolution of various functions (*e.g.*, mean square displacement to diffusion through Einstein relation). In particular, the thermal conductivity can be obtained from the equilibrium behavior of an energy moment vector, **R**

$$\mathbf{R}(t) = \sum_i \mathbf{r}_i(t)\varepsilon_i(t) \tag{2}$$

where ε_i is the energy content of atom *i*. In a nonconvective system, this energy moment expression may be expressed as[71]

$$\mathbf{R}(t) = \sum_i \mathbf{r}_i \int_0^t \mathbf{f}_i(\tau)\mathbf{v}_i(\tau)\mathrm{d}\tau \tag{3}$$

where *i* is a summation over all particles in the simulation cell as well as the images which form unique interaction groups (*i.e.*, pairs for 2-body, triplets for 3-body, *etc.*). The force on particle *i* due to all unique interactions of *i* is represented by $\mathbf{f}_i$; $\mathbf{r}_i$ and $\mathbf{v}_i$ are simply the position and velocity of the same particle. Using this definition, the thermal conductivity in a given direction, $\kappa_{\mu\nu}$, is found *via* an equation akin to the Einstein diffusion expression

$$\kappa_{\mu\nu} = \frac{1}{Vk_B T^2} \lim_{t\to\infty} \frac{1}{2t} \langle [R_\mu(t) - R_\mu(0)][R_\nu(t) - R_\nu(0)] \rangle \tag{4}$$

with *T*, k_B, and *V* being the temperature, Boltzmann constant, and volume, respectively.

Though Green–Kubo theory requires lengthy simulations to generate converged results, it provides the best representation of thermal conductivity, as the assumptions regarding phonon relaxation times, phonon velocities, and anharmonic effects required for other models are implicitly included in the temporal behavior of R_μ. The simulations performed herein use the NVE ensemble and a time step of 1 fs, the optimum step that conserves energy and reliably converges R_μ. Each data point for the thermal conductivity is obtained from the average of multiple simulations each lasting a minimum of 5 ns. A time scale on the order of a few nanoseconds is necessary to accurately average the vibrational processes that contribute to thermal conductivity. For the calculations with GNRs, we determine only the κ component along the direction of the ribbon length and define the volume as the surface area of the 2D GNR times the interplanar spacing of graphite.

For electronic transport calculations, a tight-binding (TB) model is employed together with non-equilibrium Green's functions. The tight-binding Hamiltonian is written as $H = -t\Sigma_{\langle i,j\rangle}(c_i^\dagger c_j + Hc)$, where t = 2.7 eV, $c_i^\dagger$ (c_i) is the electron creation (annihilation) operator at site *i*, and the summation runs over the first nearest neighbors.[65] The TB Hamiltonian is known to yield results in agreement with first-principles density functional theory (DFT) calculations for graphene in both one and two dimensions[72] and also in the presence of vacancies.[21] We determined the electronic band structure for pristine ZGNR-(70) as well as defective ZNGRs. Here, 70 is the number of zigzag chains in the transverse direction, and it corresponds to a width of 15 nm. Pristine ZGNR is a zero gap semiconductor independent of its width with a high density of states around the charge neutrality point (CNP). The reservoirs are modeled with semi-infinite pristine GNRs coupled to the central region from left and right, and the electronic conductance is calculated as

$$\mathscr{G}(\mu, T) = -\frac{2e^2}{h} \int_{-\infty}^{\infty} \mathrm{d}E\, \mathscr{T}(E) \frac{\partial f_F(E, \mu, T)}{\partial E} \tag{5}$$

with f_F being the Fermi distribution function, μ is the chemical potential, T is temperature and $\mathscr{T} = \mathrm{Tr}[\Gamma_L G^R \Gamma_R G^A]$ is the transmission coefficient. Here $\Gamma_{L(R)}$ stands for the broadening due to coupling to the left (right) reservoir, $G^{R(A)}$ is the retarded (advanced) GF of the central region.[73] G^R values of long ribbons are calculated using the recursion scheme.[68] We carry out calculations for 25 different realizations of disorder and perform ensemble averages. Onsager coefficients are calculated using the functions $L_n(\mu,T) = \int \mathrm{d}E(-\partial f_F(E,\mu,T)/\partial E)(E-\mu)^n \mathscr{T}(E)$.[74,75] Temperature-dependent electrical conductance is defined as $\mathscr{G}(\mu,T) = (2e^2/h)L_0$, and the Seebeck coefficient can be obtained with $S(\mu,T) = (-1/eT)L_1/L_0$. The electron and phonon contributions to thermal conductance are given with $\sigma_{el}(\mu,T) = (2/hT)(L_2 - L_1^2/L_0)$ and $\sigma_{ph} = \kappa A/L$, respectively. Here, A is the cross section area, L is length of the ribbon, and κ is the lattice thermal conductivity. Thermoelectric figure of merit is defined as $ZT = S^2\mathscr{G}T/(\sigma_{el} + \sigma_{ph})$.

In this study, we employed both classical dynamics and tight-binding model to rough ribbons which are created by randomly but continuously varying the edge profile between predefined limits. The distance between the limits, consequently, determines the roughness for an edge. In defining the roughness for the ribbons, we used a common root mean squared parameter, R_{rms}. Briefly, R_{rms} is the standard deviation of the positions of atoms at the edge from the mean of the whole edge. Since there are two edges, the total roughness is the average of these two.

Acknowledgment. J.B.H., A.K., C.S., and T.C. acknowledge support from NSF (DMR 0844082) to International Institute of Materials for Energy Conversion at Texas A&M University as well as AFRL. The parts of computations are carried out at the facilities of Laboratory of Computational Engineering of Nanomaterials also supported by ARO, ONR, and DOE grants. We also would like to thank for generous time allocation made for this project by the Supercomputing Center of Texas A&M University. H.S. and G.C. would like to acknowledge the support by the priority program Nanostructured Thermoelectrics (SPP-1386) of the German Research Foundation (DFG) (Contract No. CU 44/11-1), the cluster of excellence of the Free State of Saxony ECEMP–European Center for Emerging Materials and Processes Dresden (Project A2), and the European Social Funds (ESF) in Saxony (research group InnovaSens). G.C. further acknowledges support from the WCU (World Class University) program sponsored by the South Korean Ministry of Education, Science, and Technology Program, Project No. R31-2008-000-10100-0. The Center for Information Services and High Performance Computing (ZIH) at the TU-Dresden is also acknowledged.

REFERENCES AND NOTES

1. Geim, A. K.; Novoselov, K. S. The Rise of Graphene. *Nat. Mater.* **2007,** *6*, 183–191.
2. Geim, A. K. Graphene: Status and Prospects. *Science* **2009,** *324*, 1530–1534.
3. Castro Neto, A. H.; Guinea, F.; Peres, N. M. R.; Novoselov, K. S.; Geim, A. K. The Electronic Properties of Graphene. *Rev. Mod. Phys.* **2009,** *81*, 109–162.
4. Novoselov, K. S.; Geim, A. K.; Morozov, S. V.; Jiang, D.; Zhang, Y.; Dubonos, S. V.; Grigorieva, I. V.; Firsov, A. A. Electric Field Effect in Atomically Thin Carbon Films. *Science* **2004,** *306*, 666–669.
5. Wakabayashi, K.; Takane, Y.; Sigrist, M. Perfectly Conducting Channel and Universality Crossover in Disordered Graphene Nanoribbons. *Phys. Rev. Lett.* **2007,** *99*, 036601-4.
6. Zhang, Y.; Tan, Y.; Stormer, H.; Kim, P. Experimental Observation of the Quantum Hall Effect and Berry's Phase in Graphene. *Nature* **2005,** *438*, 201–204.
7. Cresti, A.; Nemec, N.; Biel, B.; Niebler, G.; Triozon, F.; Cuniberti, G.; Roche, S. Charge Transport in Disordered Graphene-Based Low Dimensional Materials. *Nano Res.* **2008,** *1*, 361–394.
8. Xu, X.; Gabor, N. M.; Alden, J. S.; van der Zande, A. M.; McEuen, P. L. Photo-thermoelectric Effect at a Graphene Interface Junction. *Nano Lett.* **2010,** *10*, 562–566.
9. Nair, R. R.; Blake, P.; Grigorenko, A. N.; Novoselov, K. S.; Booth, T. J.; Stauber, T.; Peres, N. M. R.; Geim, A. K. Fine Structure Constant Defines Visual Transparency of Graphene. *Science* **2008,** *320*, 1308.
10. Seol, J. H.; Jo, I.; Moore, A. L.; Lindsay, L.; Aitken, Z. H.; Pettes, M. T.; Li, X.; Yao, Z.; Huang, R.; Broido, D.; *et al.* Two-Dimensional Phonon Transport in Supported Graphene. *Science* **2010,** *328*, 213–216.
11. Balandin, A. A.; Ghosh, S.; Bao, W.; Calizo, I.; Teweldebrhan, D.; Miao, F.; Lau, C. N. Superior Thermal Conductivity of Single-Layer Graphene. *Nano Lett.* **2008,** *8*, 902–907.
12. Ghosh, S.; Bao, W.; Nika, D. L.; Subrina, S.; Pokatilov, E. P.; Lau, C. N.; Balandin, A. A. Dimensional Crossover of Thermal Transport in Few-Layer Graphene. *Nat. Mater.* **2010,** *9*, 555–558.
13. Cai, W.; Moore, A. L.; Zhu, Y.; Li, X.; Chen, S.; Shi, L.; Ruoff, R. S. Thermal Transport in Suspended and Supported Monolayer Graphene Grown by Chemical Vapor Deposition. *Nano Lett.* **2010,** *10*, 1645–1651.
14. Faugeras, C.; Faugeras, B.; Orlita, M.; Potemski, M.; Nair, R. R.; Geim, A. K. Thermal Conductivity of Graphene in Corbino Membrane Geometry. *ACS Nano* **2010,** *4*, 1889–1892.
15. Lee, C.; Wei, X.; Kysar, J. W.; Hone, J. Measurement of the Elastic Properties and Intrinsic Strength of Monolayer Graphene. *Science* **2008,** *321*, 385–388.
16. Yamada, M.; Yamakita, Y.; Ohno, K. Phonon Dispersions of Hydrogenated and Dehydrogenated Carbon Nanoribbons. *Phys. Rev. B* **2008,** *77*, 054302-13.
17. Dragoman, D.; Dragoman, M. Giant Thermoelectric Effect in Graphene. *Appl. Phys. Lett.* **2007,** *91*, 203116-3.
18. Nakada, K.; Fujita, M.; Dresselhaus, G.; Dresselhaus, M. S. Edge State in Graphene Ribbons: Nanometer Size Effect and Edge Shape Dependence. *Phys. Rev. B* **1996,** *54*, 17954–17958.
19. Son, Y.-W.; Cohen, M. L.; Louie, S. G. Half-Metallic Graphene Nanoribbons. *Nature* **2006,** *444*, 347–349.
20. Sevinçli, H.; Topsakal, M.; Ciraci, S. Superlattice Structures of Graphene-Based Armchair Nanoribbons. *Phys. Rev. B* **2008,** *78*, 245402-8.
21. Topsakal, M.; Aktürk, E.; Sevinçli, H.; Ciraci, S. First-Principles Approach To Monitoring the Band Gap and Magnetic State of a Graphene Nanoribbon *via* Its Vacancies. *Phys. Rev. B* **2008,** *78*, 235435-6.
22. Yan, Q.; Huang, B.; Yu, J.; Zheng, F.; Zang, J.; Wu, J.; Gu, B.-L.; Liu, F.; Duan, W. Intrinsic Current Voltage Characteristics of Graphene Nanoribbon Transistors and Effect of Edge Doping. *Nano Lett.* **2007,** *7*, 1469–1473.
23. Zuanyi, L.; Haiyun, Q.; Jian, W.; Bing-Lin, G.; Wenhui, D. Role of Symmetry in the Transport Properties of Graphene Nanoribbons under Bias. *Phys. Rev. Lett.* **2008,** *100*, 206802-4.
24. Rycerz, A.; Tworzydlo, J.; Beenakker, C. W. J. Valley Filter and Valley Valve in Graphene. *Nat. Phys.* **2007,** *3*, 172–175.
25. Han, M. Y.; Özyılmaz, B.; Zhang, Y.; Kim, P. Energy Band-Gap Engineering of Graphene Nanoribbons. *Phys. Rev. Lett.* **2007,** *98*, 206805-4.
26. Ghosh, S.; Calizo, I.; Teweldebrhan, D.; Pokatilov, E. P.; Nika, D. L.; Balandin, A. A.; Bao, W.; Miao, F.; Lau, C. N. Extremely High Thermal Conductivity of Graphene: Prospects for Thermal Management Applications in Nanoelectronic Circuits. *Appl. Phys. Lett.* **2008,** *92*, 151911.
27. Bae, M.-H.; Ong, Z.-Y.; Estrada, D.; Pop, E. Imaging, Simulation, and Electrostatic Control of Power Dissipation in Graphene Devices. *Nano Lett.* **2010,** *10*, 4787–4793.
28. Sevinçli, H.; Cuniberti, G. Enhanced Thermoelectric Figure of Merit in Edge-Disordered Zigzag Graphene Nanoribbons. *Phys. Rev. B* **2010,** *81*, 113401-4.
29. Zuev, Y. M.; Chang, W.; Kim, P. Thermoelectric and Magnetothermoelectric Transport Measurements of Graphene. *Phys. Rev. Lett.* **2009,** *102*, 096807-4.
30. Chen, Y.; Jayasekera, T.; Calzolari, A.; Kim, K. W.; Nardelli, M. B. Thermoelectric Properties of Graphene Nanoribbons, and Superlattices. *J. Phys.: Condens. Matter* **2010,** *22*, 372202-5.
31. Ni, X.; Liang, G.; Wang, J.-S.; Li, B. Disorder Enhances Thermoelectric Figure of Merit in Armchair Graphane Nanoribbons. *Appl. Phys. Lett.* **2009,** *95*, 192114-3.
32. Sim, D.; Liu, D.; Dong, X.; Xiao, N.; Li, S.; Zhao, Y.; Li, L.-J.; Yan, Q.; Hng, H. H. Power Factor Enhancement for Few-Layered Graphene Films by Molecular Attachments. *J. Phys. Chem. C* **2011,** *115*, 1780–1785.
33. Li, X.; Wang, X.; Zhang, L.; Lee, S.; Dai, H. Chemically Derived, Ultrasmooth Graphene Nanoribbon Semiconductors. *Science* **2008,** *319*, 1229–1232.
34. Jiao, L.; Zhang, L.; Wang, X.; Diankov, G.; Dai, H. Narrow Graphene Nanoribbons from Carbon Nanotubes. *Nature* **2009,** *458*, 877–880.
35. Cai, J.; Ruffieux, P.; Jaafar, R.; Bieri, M.; Braun, T.; Blankenburg, S.; Muoth, M.; Seitsonen, A. P.; Saleh, M.; Feng, X.; *et al.* Atomically Precise Bottom-Up Fabrication of Graphene Nanoribbons. *Nature* **2010,** *466*, 470–473.
36. Kong, B. D.; Paul, S.; Nardelli, M. B.; Kim, K. W. First-Principles Analysis of Lattice Thermal Conductivity in Monolayer and Bilayer Graphene. *Phys. Rev. B* **2009,** *80*, 033406-4.
37. Nika, D. L.; Pokatilov, E. P.; Askerov, A. S.; Balandin, A. A. Phonon Thermal Conduction in Graphene: Role of Umklapp and Edge Roughness Scattering. *Phys. Rev. B* **2009,** *79*, 155413-12.
38. Lindsay, L.; Broido, D. A. Optimized Tersoff and Brenner Empirical Potential Parameters for Lattice Dynamics and Phonon Thermal Transport in Carbon Nanotubes and Graphene. *Phys. Rev. B* **2010,** *81*, 205441-6.
39. Saito, K.; Nakamura, J.; Natori, A. Ballistic Thermal Conductance of a Graphene Sheet. *Phys. Rev. B* **2007,** *76*, 115409-4.
40. Evans, W. J.; Hu, L.; Keblinski, P. Thermal Conductivity of Graphene Ribbons from Equilibrium Molecular Dynamics: Effect of Ribbon Width, Edge Roughness, and Hydrogen Termination. *Appl. Phys. Lett.* **2010,** *96*, 203112-3.
41. Lan, J.; Wang, J.-S.; Gan, C. K.; Chin, S. K. Edge Effects on Quantum Thermal Transport in Graphene Nanoribbons: Tight-Binding Calculations. *Phys. Rev. B* **2009,** *79*, 115401-5.
42. Ouyang, T.; Chen, Y. P.; Yang, K. K.; Zhong, J. X. Thermal Transport of Isotopic-Superlattice Graphene Nanoribbons with Zigzag Edge. *EPL* **2009,** *88*, 28002-5.
43. Guo, Z.; Zhang, D.; Gong, X.-G. Thermal Conductivity of Graphene Nanoribbons. *Appl. Phys. Lett.* **2009,** *95*, 163103-3.
44. Muñoz, E.; Lu, J.; Yakobson, B. I. Ballistic Thermal Conductance of Graphene Ribbons. *Nano Lett.* **2010,** *10*, 1652–1656.

45. Hu, J.; Ruan, X.; Chen, Y. P. Thermal Conductivity and Thermal Rectification in Graphene Nanoribbons: A Molecular Dynamics Study. *Nano Lett.* **2009,** *9*, 2730–2735.
46. Yamamoto, T.; Watanabe, K.; Mii, K. Empirical-Potential Study of Phonon Transport in Graphitic Ribbons. *Phys. Rev. B* **2004,** *70*, 245402-7.
47. Yang, N.; Zhang, G.; Li, B. Thermal Rectification in Asymmetric Graphene Ribbons. *Appl. Phys. Lett.* **2009,** *95*, 033107-3.
48. Li, W.; Sevinçli, H.; Cuniberti, G.; Roche, S. Phonon Transport in Large Scale Carbon-Based Disordered Materials: Implementation of an Efficient Order-*N* and Real-Space Kubo Methodology. *Phys. Rev. B* **2010,** *82*, 041410-4.
49. Tan, Z. W.; Wang, J.-S.; Gan, C. K. First-Principles Study of Heat Transport Properties of Graphene Nanoribbons. *Nano Lett.* **2011,** *11*, 214–219.
50. Yong, X.; Xiaobin, C.; Bing-Lin, G.; Wenhui, D. Intrinsic Anisotropy of Thermal Conductance in Graphene Nanoribbons. *Appl. Phys. Lett.* **2009,** *95*, 233116-3.
51. Areshkin, D. A.; Gunlycke, D.; White, C. T. Ballistic Transport in Graphene Nanostrips in the Presence of Disorder: Importance of Edge Effects. *Nano Lett.* **2007,** *7*, 204–210.
52. Lherbier, A.; Biel, B.; Niquet, Y.-M.; Roche, S. Transport Length Scales in Disordered Graphene-Based Materials: Strong Localization Regimes and Dimensionality Effects. *Phys. Rev. Lett.* **2008,** *100*, 036803-3.
53. Mucciolo, E. R.; Castro Neto, A. H.; Lewenkopf, C. H. Conductance Quantization and Transport Gaps in Disordered Graphene Nanoribbons. *Phys. Rev. B* **2009,** *79*, 075407-5.
54. Dubois, S. M.-M.; Lopez-Bezanilla, A.; Cresti, A.; Triozon, F.; Biel, B.; Charlier, J.-C.; Roche, S. Quantum Transport in Graphene Nanoribbons: Effects of Edge Reconstruction and Chemical Reactivity. *ACS Nano* **2010,** *4*, 1971–1976.
55. Libisch, F.; Rotter, S.; Burgdörfer, J. Transport through Graphene Nanoribbons: Suppression of Transverse Quantization by Symmetry Breaking. *J. Phys.: Condens. Matter* 2011, arXiv:1102.03848v1.
56. Basu, D.; Gilbert, M. J.; Register, L. F.; Banerjee, S. K.; MacDonald, A. H. Effect of Edge Roughness on Electronic Transport in Graphene Nanoribbon Channel Metal-Oxide-Semiconductor Field-Effect Transistors. *Appl. Phys. Lett.* **2008,** *92*, 042114-3.
57. Querlioz, D.; Apertet, Y.; Valentin, A.; Huet, K.; Bournel, A.; Galdin-Retailleau, S.; Dollfus, P. Suppression of the Orientation Effects on Bandgap in Graphene Nanoribbons in the Presence of Edge Disorder. *Appl. Phys. Lett.* **2008,** *92*, 042108-3.
58. Li, W.; Sevinçli, H.; Roche, S.; Cuniberti, G. Efficient Linear Scaling Method for Computing the Thermal Conductivity of Disordered Materials. *Phys. Rev. B* **2011,** *83*, 155416–155419.
59. Wakabayashi, K.; Takane, Y.; Sigrist, M. Perfectly Conducting Channel and Universality Crossover in Disordered Graphene Nanoribbons. *Phys. Rev. Lett.* **2007,** *99*, 036601-4.
60. Ihnatsenka, S.; Kirczenow, G. Conductance Quantization in Strongly Disordered Graphene Ribbons. *Phys. Rev. B* **2009,** *80*, 201407-4.
61. Lin, Y.-M.; Perebeinos, V.; Chen, Z.; Avouris, P. Electrical Observation of Subband Formation in Graphene Nanoribbons. *Phys. Rev. B* **2008,** *78*, 161409-4.
62. Tersoff, J. Modeling Solid-State Chemistry: Interatomic Potentials for Multicomponent Systems. *Phys. Rev. B* **1989,** *39*, 5566–5568.
63. Wang, Z.; Xie, R.; Bui, C. T.; Liu, D.; Ni, X.; Li, B.; Thong, J. T. L. Thermal Transport in Suspended and Supported Few-Layer Graphene. *Nano Lett.* **2011,** *11*, 113–118.
64. Che, J.; Çağın, T.; Goddard, W. Thermal Conductivity of Carbon Nanotubes. *Nanotechnology* **2000,** *11*, 65–69.
65. Fujita, M.; Wakabayashi, K.; Nakada, K.; Kusakabe, K. Peculiar Localized State at Zigzag Graphite Edge. *J. Phys. Soc. Jpn.* **1996,** *65*, 1920–1923.
66. Datta, S.; Cahay, M.; McLennan, M. Scatter-Matrix Approach to Quantum Transport. *Phys. Rev. B* **1987,** *36*, 5655–5658.
67. Markussen, T.; Rurali, R.; Jauho, A.-P.; Brandbyge, M. Scaling Theory Put into Practice: First-Principles Modeling of Transport in Doped Silicon Nanowires. *Phys. Rev. Lett.* **2007,** *99*, 076803-4.
68. Sancho, M. P. L.; Sancho, J. M. L.; Sancho, J. M. L.; Rubio, J. Highly Convergent Schemes for the Calculation of Bulk and Surface Green Functions. *J. Phys. F: Metal Phys.* **1985,** *15*, 851–858.
69. Carruthers, P. Theory of Thermal Conductivity of Solids at Low Temperatures. *Rev. Mod. Phys.* **1961,** *33*, 92–138.
70. Kubo, R. Statistical-Mechanical Theory of Irreversible Processes. I. General Theory and Simple Applications to Magnetic and Conduction Problems. *J. Phys. Soc. Jpn.* **1957,** *12*, 570–586.
71. Kinaci, A.; Haskins, J. B.; Çağın, T. Evaluation of Energy Moment in Solid Systems. *J. Chem. Phys.* Submitted for publication.
72. Son, Y.-W.; Cohen, M. L.; Louie, S. G. Energy Gaps in Graphene Nanoribbons. *Phys. Rev. Lett.* **2006,** *97*, 216803-4.
73. Datta, S. *Electronic Transport in Mesoscopic Systems*; Cambridge University Press: Cambridge, 1995.
74. Lunde, A. M.; Flensberg, K. On the Mott Formula for the Thermopower of Non-interacting Electrons in Quantum Point Contacts. *J. Phys.: Condens. Matter* **2005,** *17*, 3879–3884.
75. Zheng, X.; Zheng, W.; Wei, Y.; Zeng, Z.; Wang, J. Thermoelectric Transport Properties in Atomic Scale Conductors. *J. Chem. Phys.* **2004,** *121*, 8537–8541.